ChemPubSoc Europe

DOI: 10.1002/cphc.201600948

CHEMPHYSCHEM Articles

Is Steam an Oxidant or a Reductant for Nickel/Doped-Ceria Cermets?

Vasiliki Papaefthimiou,[a] Dimitris K. Niakolas,[b] Fotios Paloukis,[a] Thierry Dintzer,[a] and Spyridon Zafeiratos*[a]

Nickel/doped-ceria composites are promising electrocatalysts for solid-oxide fuel and electrolysis cells. Very often steam is present in the feedstock of the cells, frequently mixed with other gases, such as hydrogen or CO_2. An increase in the steam concentration in the feed mixture is considered accountable for the electrode oxidation and the deactivation of the device. However, direct experimental evidence of the steam interaction with nickel/doped-ceria composites, with adequate surface specificity, are lacking. Herein we explore in situ the surface state of nickel/gadolinium-doped ceria (NiGDC) under O_2, H_2, and H_2O environments by using near-ambient-pressure X-ray photoelectron and absorption spectroscopies. Changes in the surface oxidation state and composition of NiGDC in response to the ambient gas are observed. It is revealed that, in the mbar pressure regime and at intermediate temperature conditions (500–700 °C), steam acts as an oxidant for nickel but has a dual oxidant/reductant function for doped ceria.

1. Introduction

Nickel/doped-ceria ceramic–metal composite materials (cermets) find important applications in energy conversion devices, notably in solid-oxide-cell (SOC) systems. SOCs can operate as both a fuel cell (SOFC) to generate electricity by using stored fuels and an electrolysis cells (SOEC) to convert electricity into fuels.[1,2,3] Of all the doped-ceria types, Gd-doped ceria ($Ce_{0.9}Gd_{0.1}O_{1.95}$, GDC) exhibits one of the highest ionic conductivities and good application potential.[4–6] The addition of nickel provides adequate electronic conductivity and a high catalytic activity in the cermet, even at intermediate temperatures. Incorporation of GDC within the anode electrode of SOFCs prevents carbon deposition, which is a dominant factor for cell degradation.[7,8] In addition, NiGDC cathodes improve the performance of SOECs devices compared with that of Ni–yttria-stabilized zirconia (Ni-YSZ) electrodes.[9–11]

One of the important benefits of SOCs is their high fuel-feed flexibility, which extends from hydrogen and water to oxygenated hydrocarbons.[12] Water, in the form of steam, is ubiquitous in almost all SOC applications as a reactant, a product, or simply as part of the ambient atmosphere. For example, in the fuel-cell mode, humidified methane or hydrogen fuels are fed in the anode and react with oxygen ions to form CO_2 and water.[13] In addition, steam is introduced in the cathode of both water and CO_2 electrolysis cells to produce hydrogen.[14] Therefore, it is evident that under these operating conditions, the NiGDC–steam interaction will influence the redox stability and performance of the device.

The reactivity of water with nickel and ceria surfaces has been investigated separately in a great number of studies; many of these have been carried out under ultra-high vacuum (UHV) conditions. Polycrystalline nickel is oxidized to NiO by water vapor, but at a slower rate than by O_2.[15] Interestingly, the reverse reaction, that is, reduction of NiO to Ni in the presence of water, has been also reported.[16] Model Ni-YSZ electrodes in equilibrium with 0.4 mbar H_2/H_2O mixtures were investigated by using near-ambient pressure X-ray photoelectron spectroscopy (NAP-XPS) at 700 °C. Under these conditions, the nickel remained metallic, whereas oxidation was reported only after bias.[17]

Well-defined model ceria surfaces exposed to water vapor have been extensively studied by using both computational and experimental approaches.[18–20] It is generally concluded that water can be dissociatively adsorbed on both reduced and stoichiometric ceria surfaces, whereas this process is promoted by the presence of vacancies on reduced ceria. In H_2/H_2O mixtures, ceria is reduced to a mixed-valence-state CeO_x ($1.5 < x < 2$), which represents an intermediate case between CeO_2 and Ce_2O_3 oxides.[21,22]

Separate studies of nickel and ceria interactions with steam do not account for the potential influence of their synergy; however, reports on mixed Ni–CeO_2 compounds are scarce. In a recent study, Carrasco et al. found that water dissociation on model Ni–CeO_2 (111) catalysts is more efficient than on bare ceria supports.[23] In addition, by using in situ Raman spectroscopy, it was shown that, under a humidified H_2 atmosphere,

[a] Dr. V. Papaefthimiou, Dr. F. Paloukis, Dr. T. Dintzer, Dr. S. Zafeiratos
Institut de Chimie et Procédés pour l'Energie
l'Environnement et la Santé (ICPEES), ECPM
UMR 7515 CNRS-Université de Strasbourg
25, rue Becquerel, 67087 Strasbourg Cedex 02 (France)
E-mail: spiros.zafeiratos@unistra.fr

[b] D. K. Niakolas
FORTH/ICE-HT
26504 Rion, Patras (Greece)

Supporting Information and the ORCID identification number(s) for the author(s) of this article can be found under http://dx.doi.org/10.1002/cphc.201600948.

the oxidation state of GDC in NiGDC cermets is stabilized at a higher valence than under dry H_2.[24] Apparently, it is difficult to isolate the effect of water on oxidation from studies performed under H_2/H_2O mixtures, due to the presence of the highly reductive H_2. However, it is evident that NiGDC cermets are not static and may continually undergo phase transformations in response to variations in temperature, gas composition, and pressure.

Herein, we explored the surface state of NiGDC prepared as a SOC electrode under O_2, H_2, and H_2O gas atmospheres and at intermediate temperature conditions. The dynamic surface state and composition of the electrode in response to the ambient gas was revealed in situ by using near-ambient pressure photoelectron and near-edge absorption fine structure spectroscopies (NAP-XPS and NEXAFS, respectively).

2. Results and Discussion

2.1. NiGDC in an O_2 Atmosphere

The surface state of the NiGDC electrode in equilibrium with 0.2 mbar O_2 was investigated first. Figure 1a and b shows the Ce 3d/Ni 2p NAP-XPS peaks for NiGDC at 500 and 700 °C after about 20 min under O_2. In addition, the spectra of reference CeO_2 and NiO compounds recorded under identical conditions

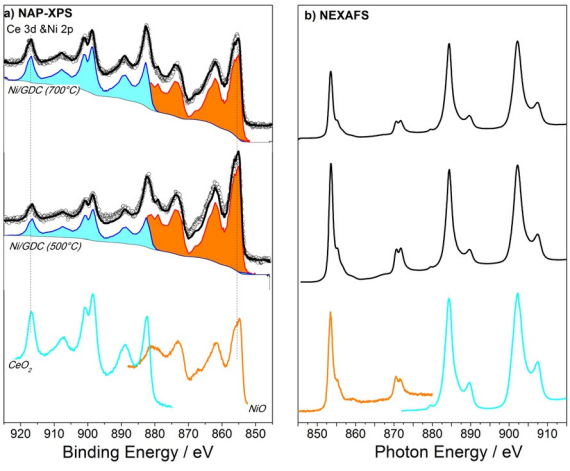

Figure 1. a) Ce 3d/Ni 2p ($h\nu = 1065$ eV) NAP-XPS spectra. b) Ni $L_{3,2}$- and Ce $M_{5,4}$-edge NEXAFS spectra. The measurement conditions were 0.2 mbar O_2 at 700 (top) and 500 °C (middle). The measured Ce 3d/Ni 2p spectrum (○) is well fitted (——) by a linear combination of the reference CeO_2 and NiO spectra (bottom) measured from standard powder samples under similar acquisition conditions.

are included for comparison. The Ce 3d spectrum of the CeO_2 reference powder (Figure 1a, bottom spectrum), has three pairs of spin-orbit doublets and a characteristic intense peak at approximately 917 eV, in full agreement with previous reports.[25] Similarly, the Ni 2p reference peak, which is centered at 855.5 eV and is accompanied by a satellite peak shifted by 6.2 eV at higher binding energies, indicates NiO formation.[26,27] Apparently, analysis of the Ce 3d/Ni 2p spectra of the NiGDC sample is quite complex because a variety of structures due to initial and final state effects, which include chemical shifts, asymmetric peaks, spin-orbit coupling, multiplet splitting, and shake-up satellites, co-exist in a quite narrow energy range.[28] In addition, the Ni $2p_{1/2}$ and Ce $3d_{5/2}$ photoelectron peaks partly overlap, which further complicates the peak assignment. The use of individual peaks to fit the overall spectrum is complex and results in highly correlated parameters. An alternative approach to fit the Ce 3d and Ni 2p spectra is to use spectra from standards as the basis functions for linear peak fitting. This approach was followed here and, as shown in Figure 1a, the overall spectrum at both temperatures could be suitably fitted by the reference spectra recorded for standard CeO_2 and NiO powder samples. This affirms that, under O_2, the surface of NiGDC cermet was readily oxidized to a mixture of NiO and CeO_2 without any evident temperature effect. Please note that the enhanced Ni 2p peak intensity at 500 °C, compared with that at 700 °C, suggests that a lower temperature favors the presence of nickel at the surface.

The Ni L_3- and Ce M_5-edge NEXAFS lines (Figure 1b) can be used to validate the NAP-XPS results because the CeO_2 and NiO NEXAFS peaks are well separated, as shown in Figure 1, bottom. In addition, due to the higher analysis depth of NEXAFS in total-electron-yield (TEY) mode, compared with NAP-XPS (4 or 5 nm instead of 1.7 nm),[29] the NEXAFS results can be used to conclude whether oxidation is also propagated in deeper layers or whether it is restricted to the outer surface. The NEXAFS spectra of NiGDC and the reference NiO and CeO_2 samples show a great resemblance, which confirms the NAP-XPS results and indicates that the oxidation propagated at least in the outer 4 nm. It is interesting to note that the relative intensity of the NiO NEXAFS peak is enhanced at 500 °C compared with that of CeO_2, similar to the observations in the NAP-XPS results. Overall, the spectroscopic results show that the NiGDC cermet surface was readily oxidized in O_2 without evident differences at the two examined temperatures.

2.2. NiGDC in an H_2 Atmosphere

Figure 2 shows the spectroscopic results for the reduction of oxidized NiGDC under 0.2 mbar H_2 at two temperatures. The changes in the Ce 3d and Ni 2p peak positions and shapes, shown in Figure 2a, indicate that the oxide film underwent oxidation state changes in H_2. In particular, the Ni 2p peak shifts to 852.6 eV and the intensity of the accompanying satellite peak decreases considerably, which demonstrates the reduction of NiO to metallic Ni.[30,27,31] The similarities between NiGDC and the reference metallic Ni 2p spectra shown in Figure 2a, bottom, suggest that the reduction of NiO in NiGDC was complete at both examined temperatures. Moreover, the Ce 3d region under H_2 is also markedly modified compared with the O_2 environment. Notably, the intensity of the peak at approximately 917 eV, characteristic of Ce^{4+}, decreases and new peaks at around 905 and 886.4 eV appear due to Ce^{3+} formation.[32] Similar spectra modifications were also observed for the reference ceria powder spectrum (Figure 2a, bottom). Please note that at 700 °C under H_2, the ceria powder was not completely reduced and, therefore, the reference $CeO_{1.5}$ spec-

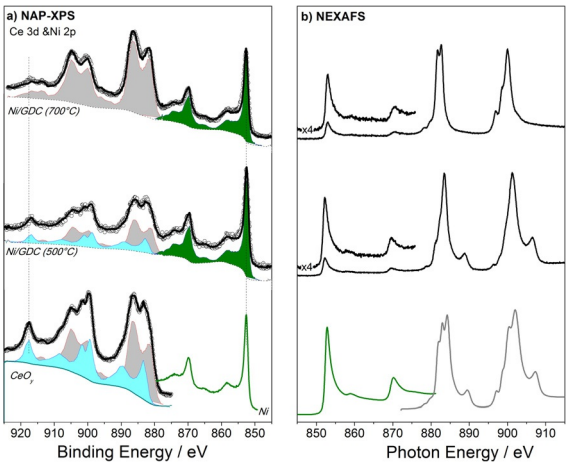

Figure 2. a) Ce 3d/Ni 2p ($h\nu = 1065$ eV) NAP-XPS spectra b) Ni $L_{3,2}$- and Ce $M_{5,4}$-edge NEXAFS spectra. The Ni $L_{3,2}$-edge is magnified four times. The measurement conditions were 0.2 mbar H_2 at 700 (top) and 500 °C (middle). The measured Ce 3d/Ni 2p spectrum (○) is well fitted (——) by a linear combination of the reference $CeO_{1.5}$ and metallic Ni spectra (bottom) measured from standard powder samples under similar acquisition conditions.

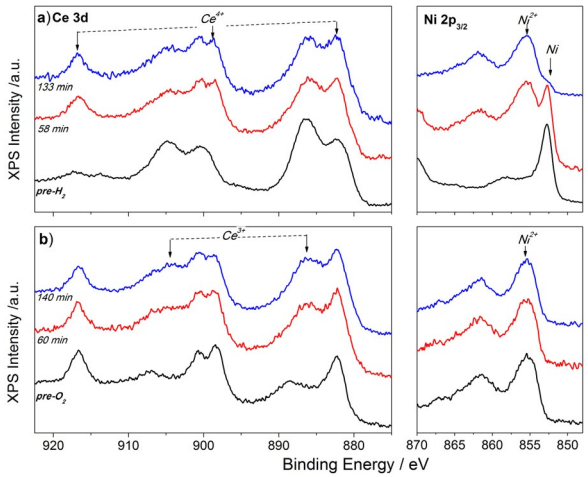

Figure 3. a) Ce 3d and Ni $2p_{3/2}$ ($h\nu = 1065$ eV) NAP-XPS spectra for the NiGDC electrode recorded at 700 °C after various H_2O exposure periods; a) electrode pretreated in H_2, b) electrode pretreated in O_2.

trum was taken from our earlier publication on NiGDC.[30] The fitting procedure of the NAP-XPS Ce 3d peak reveals that at 700 °C ceria was transformed to Ce^{3+}, whereas at 500 °C the Ce 3d spectrum contains about 25% unreduced Ce^{4+}. The oxidation state of cerium changed rapidly after contact with H_2, and was not modified further after a prolonged stay under the given ambient atmosphere (see Supporting Information 1).

The NAP-XPS results are fully supported by the NEXAFS spectra shown in Figure 2b. The Ce M-edge at 700 °C is in good agreement with the recently published Ce^{3+} NEXAFS spectra,[30,33] whereas at 500 °C the Ce M-edge is a superimposition of the Ce^{4+} and Ce^{3+} spectral features. Finally, the Ni L-edge is the same at both temperatures and corresponds to metallic nickel.[30] A comparison of the Ce 3d and Ce M-edge spectra for NiGDC and the standard ceria powder sample recorded under identical conditions demonstrates that the ceria in NiGDC is significantly more reduced. The addition of Gd^{3+} dopant into ceria was not expected to influence the redox properties of ceria substantially.[34] Therefore, the enhanced reducibility of ceria in NiGDC cermet as compared with ceria powder should be attributed to H_2 dissociation over nickel, as has been also proposed in recent Raman studies.[24]

The Gd valence was monitored under both oxidative and reducing conditions by recording the Gd 4d photoelectron peak. As shown in Supporting Information 2, the shape and binding energy of the Gd $4d_{5/2}$ peak at 142.4 eV are in good agreement with previous reports for Gd in the Gd^{3+} valence state.[35,36] The Gd 4d spectrum was not influenced by the gas atmosphere or the temperature, which indicates that the Gd valence remains unaffected by the redox treatment.

2.3. NiGDC in a Steam Atmosphere

As shown above, under ambient H_2 the surface reduction was rapid because the spectrum was modified within 5 min after contact with the gas and then remained stable. In contrast, when the NiGDC cermet was exposed to water vapor, the adjustment of the surface oxidation state to the gas environment was much slower. In Figure 3, the Ce 3d and Ni $2p_{3/2}$ spectra of NiGDC pretreated under H_2 (Figure 3a) or O_2 (Figure 3b) and then exposed to 0.2 mbar of H_2O vapor at 700 °C are shown for different H_2O timespans. When prereduced NiGDC was exposed to steam (Figure 3a), an additional Ni $2p_{3/2}$ peak appeared at the high binding-energy side, due to oxidized or hydroxylated nickel species. From the shape of the Ni 2p peak, it is evident that after about 2 h in steam, only a small amount of nickel (≈10%) remained in the metallic state. The remaining nonoxidized Ni can be rationalized by considering the kinetic limitations of the experiment, which are related to the low-pressure steam conditions. Note that it is not straightforward to distinguish between oxide (NiO) and hydroxide ($Ni(OH)_2$ or NiOOH) nickel species in the Ni 2p spectrum because their binding energies overlap and they all have very similar satellite peak features.[27] Additional information is provided below based on analysis of the O 1s peak.

The Ce 3d spectrum is characterized by progressive growth of the peak at 917 eV, which is associated with CeO_2 formation. After about 2 h under steam, the Ce 3d spectrum corresponded to an overlap of the CeO_2 and $CeO_{1.5}$ reference spectra, which suggests the coexistence of these two states. Moreover, a similar ceria valence was also obtained in prereduced samples under steam at lower temperature (see Supporting Information 3). Oxidation of a reduced ceria ($CeO_{1.5}$) surface by water molecules has been proposed to take place through the interaction of H_2O with oxygen vacancies.[18]

For the pre-oxidized NiGDC (Figure 3b), exposure to steam modified the Ce 3d spectrum, whereas the Ni $2p_{3/2}$ peak was practically unaffected. The intensity increase in the Ce 3d peak components at approximately 886 and 904 eV was associated with the Ce^{3+} state. This suggests that oxidized stoichiometric GDC can be partly reduced by steam under the applied conditions. Reduction of ceria surfaces during water adsorption has

been reported previously for planar single-crystalline films,[20,37] but has not been explored yet for NiGDC cermets. This is probably because the concentration of Ce^{3+} ions is limited and they are primarily located at the surface rather than the bulk ceria,[38] which makes their detection by using post-mortem analysis difficult, particularly when non-surface-sensitive methods are used.

With regard to the mechanism of ceria reduction in steam, it is unlikely that it is just a thermal effect due to the low oxygen partial pressure and the high temperature. If this was the case, then NiO would have been reduced before ceria, as has been shown previously in temperature-programmed reduction (TPR) experiments in H_2.[39] To confirm that the ceria reduction is induced by steam and is not just an effect of the low partial pressure, NiGDC was annealed stepwise under UHV pressure conditions ($<1\times10^{-7}$ mbar) at temperatures up to 600 °C (see Supporting Information 4). From these experiments, it became evident that it is possible to decompose NiO even at 400 °C, whereas GDC remained fully oxidized up to the maximum annealing temperature. Therefore, it is clear that the ceria surface reduction under steam is not a thermal effect but arises from processes similar to those reported by Henderson et al.[20] for model CeO_2 surfaces. According to these studies, adsorbed water or hydroxyl species is the driving force that leads to the migration of oxygen vacancies from the bulk ceria to its surface and induces surface reduction. Alternatively, dissociatively adsorbed water molecules on ceria can react and remove ceria lattice oxygen by releasing O_2 and H_2 in the gas phase.

The overall surface stoichiometry of nickel (x) and ceria (y) during exposure to steam was estimated by fitting the Ni 2p and Ce 3d photoelectron peaks with spectra recorded for reference materials (see Supporting Information 5). The evolution of the oxidation state as a function of time (Figure 4a and b) shows that the oxidation and reduction kinetics of ceria and nickel are very different. In prereduced NiGDC, ceria was oxidized rapidly but prolonged exposure did not induce further oxidation. Conversely, about 30% of the nickel was transformed to NiO just after exposure, but further oxidation was slow and progressed at a linear rate. Moreover, on preoxidized NiGDC, reduction of CeO_2 followed an exponential decay function, whereas, as stated above, NiO was not influenced. Overall, independent of the prior oxidation state, a mean ceria valence of $CeO_{1.72}$ could be approximated at equilibrium with water vapor, whereas the majority of nickel was converted to nickel oxide. In addition, no induction period was detected, which is probably related to the relatively high temperature.[40]

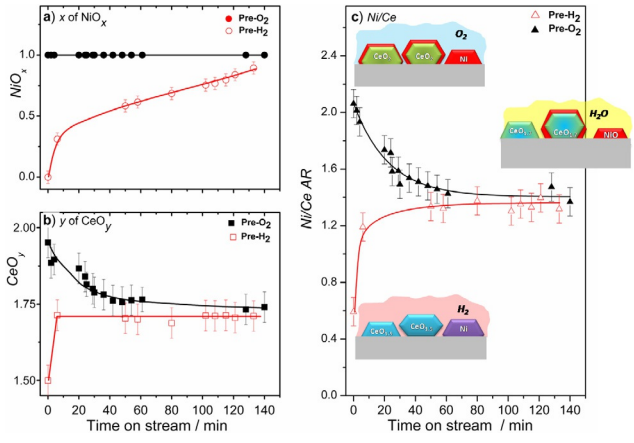

Figure 4. Isothermal time evolution of a) NiO_x and b) CeO_y surface stoichiometry and c) the Ni/Ce atomic ratio calculated from the Ni 2p and Ce 3d NAP-XPS spectra. The black (solid) and red (open) symbols represent the preoxidized and prereduced samples, respectively. Insets: Schematics of the proposed surface configuration, which comply with experimental observations. For clarity, modifications in the ceria and nickel volumes due to valence changes are not illustrated.

The Ni 2p and Ce 3d peak-area ratio (Ni/Ce AR) can be used to estimate the relative amounts of ceria and nickel exposed on the surface[41,42] and consequently to monitor the surface transformations that take place when the sample is in contact with steam. For example, shrinkage, agglomeration, or inner diffusion of nickel in ceria would be illustrated by a decrease in the Ni/Ce ratio. As shown in Figure 4c, the line profile of the Ni/Ce AR follows that of the oxidation state of ceria and is independent of that of nickel for both pretreatments. In particular, exposure of the preoxidized sample in water was followed by a gradual decay in the Ni/Ce ratio, whereas the prereduced sample followed the reverse path, that is, the Ni/Ce AR sharply increased in the first few minutes and remained almost constant thereafter. Please note that, in the latter case, nickel was gradually oxidized without significant restructuring of the electrode morphology according to the Ni/Ce AR. It is also evident that at equilibrium (after about 1 h in steam), the actual surface composition was not influenced by the pretreatment process because, as shown in Figure 4c, the Ni/Ce AR is very similar for the two cases.

The observed evolution of the Ni/Ce AR can be rationalized by taking into account the initial arrangement of nickel and ceria on the surface of NiGDC just before steam exposure. As has been reported earlier[30] for oxidized samples, stoichiometric ceria is partially covered by a thin NiO layer. This is also reflected here by the higher initial Ni/Ce ratio in the preoxidized sample shown in Figure 4c. To react with H_2O and to be reduced, CeO_2 should diffuse within the NiO layer towards the surface. Alternatively, water molecules might diffuse through the NiO layer towards ceria, reduce it and drive it to the surface. Reduction of CeO_2 to $CeO_{1.5}$ is followed by an expansion in the ceria volume (≈4–9%).[43] Both processes (ceria surface segregation and volume increase) enhance the Ce 3d NAP-XPS signal and lead to the observed progressive drop in the Ni/Ce AR measured in H_2O (Figure 4c).

In reduced NiGDC there is no evident surface segregation between nickel and ceria, as reported in our previous study.[30] Therefore, when the prereduced sample was exposed to H_2O vapor, $CeO_{1.5}$ and Ni areas were directly and rapidly oxidized to $CeO_{1.7}$ and NiO (Figure 4b). Similar to the O_2-treated sample, this was followed by rapid segregation of oxidized nickel over ceria areas, followed by a volume expansion of nickel[44] and consequently by an increase in the Ni/Ce AR. Please note that after about 50 min in steam, after which 60% of Ni was transformed to NiO (Figure 4a), the Ni/Ce ratio was practically stable (Figure 4c). This shows that nickel oxidation is restricted to the

surface and the overall volume expansion of nickel areas is limited.

Overall, the kinetics of the surface transformation upon reduction and oxidation, as expressed by the evolution of Ni/Ce ARs, seem to be primarily dictated by the oxidation state of ceria.[45] However, from the discussion above it is evident that in the long term, the pretreatment has a limited effect on the outermost surface of the electrode, which under our conditions is largely defined by its contact with steam.

2.4. Excess Surface Oxygen and Its Dependence on the Gas Atmosphere

Figure 5 shows the O 1s spectra obtained for NiGDC at 700 °C and for the reference samples under various gas atmospheres.

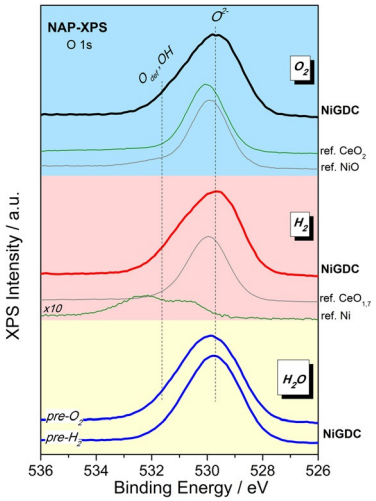

Figure 5. O 1s ($h\nu = 710$ eV) NAP-XPS spectra recorded at 700 °C in O_2, H_2, and H_2O atmospheres (from top to bottom) for NiGDC (——) and reference nickel and ceria powder samples (——).

The O 1s peak of NiGDC in O_2 is found at 529.7 eV, which is only slightly shifted relative to the reference CeO_2 and NiO powder oxides (530.0 and 529.9 eV respectively). Similar O 1s peak features were observed in a H_2 atmosphere, in which a peak shoulder at about 531.5 eV is clearly visible in the spectrum. The O 1s peak in H_2O (after 130 min) appears at 529.9 ± 0.2 eV and its shape and position is not particularly influenced by pretreatment. Evidently, the full width at half maximum (FWHM) of the O 1s peak for NiGDC and reference oxides is significantly different. In particular, the FWHM increases from 1.7 eV in the reference oxides to about 2.3 eV in NiGDC cermet. Because the two reference nickel and ceria oxides have similar O 1s binding energies, it is unlikely that the peak broadening is induced by their relative contributions in the overall O 1s spectrum. Accordingly, the origin of the larger O 1s FWHM in the NiGDC might be the higher heterogeneity of the type of oxygen ions. In particular, the shift from the main O 1s binding energy may be induced by vacancy-related defects created by doping or due to a higher amount of adsorbed hydroxyl species.[15,25,27]

Given that the OH^- species of nickel hydroxides are reported typically above 531 eV,[15,27,46] and in the spectra in Figure 5 there is only a minor contribution in this region, extensive nickel hydroxide formation is not supported. However, this does not necessarily rule out the induction of O 1s peak asymmetry by the presence of hydroxyl groups that remain adsorbed on the NiGDC surface, as proposed earlier in model ceria layer studies.[25] Depth-dependent NAP-XPS measurements can be used to distinguish between defective/interstitial lattice sites, which should be enhanced at higher analysis depth, and surface-adsorbed hydroxyl species, which should increase at lower analysis depth.[47] As shown in Supporting Information 6, the O 1s peak shape is not particularly influenced by the excitation photon energy, that is, the measurement information depth. Accordingly, the presence of a significant population of adsorbed oxygen species (i.e. hydroxyls) is not supported. Therefore, we can exclude the possibility that the O 1s peak asymmetry is due to adsorbed hydroxyls and we attribute it to defects in the ceria lattice, presumably induced by oxygen vacancies.

The absence of a significant population of adsorbed hydroxyl groups shows that the stability of these species is very poor at SOC operation temperatures, even in a steam atmosphere. This suggests that hydroxyl groups recombine fast and are removed from the surface as H_2O or dissociate further to H_2. The thermodynamics and kinetics of these reaction paths have been computed and discussed in detail by Wolverton and coworkers.[48] According to their findings, we can argue that hydroxyl decomposition into hydrogen can be facilitated over NiGDC compared with the pure ceria phase.

Overall, the presented results show the dynamic interplay of the surface state and segregation towards different stimuli (changes in the ambient gas or temperature). Although the oxidation of reduced NiGDC cermet in steam is well established,[9] the reducing effect of steam on the GDC surface is not usually considered. This can be partially explained by the fact that in most cases steam is co-fed into the cermet electrode with strong reducing agents, such as H_2 or CO. Comprehension of the interaction of steam with NiGDC surfaces is a crucial step toward the development of efficient SOC devices.

3. Conclusions

The surface state of NiGDC was found to change readily in response to the gas atmosphere and the temperature. Under 0.2 mbar O_2, full oxidation of cerium and nickel occured rapidly, driving NiO over ceria areas. Under 0.2 mbar H_2, complete reduction of NiO to metallic Ni and partial reduction of ceria were observed. A higher operation temperature seemed to promote the reduction of Ce^{4+} to Ce^{3+}. The NiGDC surface adapted to the steam atmosphere by changing its surface oxidation state and composition, but with slow kinetics compared with a H_2 or O_2 atmosphere. Under the applied steam exposure conditions, the surface was gradually transformed to NiO/$CeO_{1.7}$ independent of the NiGDC pretreatment. In addition, the surface of doped ceria was dominated by defect lattice sites (oxygen vacancies) without any evidence of adsorbed hy-

droxyl species. It is remarkable that steam may act as both an oxidant and reductant for the ceria surface, which indicates the existence of a variety of surface ceria sites with different redox chemistry on NiGDC.

Experimental Section

For the preparation of the NiGDC cermet, a procedure typically used in the manufacture of solid-oxide electrode assemblies was followed.[49,50] A slurry containing the $NiO/Gd_{0.1}Ce_{0.9}O_{1.95}$ powder (81/19 at.% ratio; Marion Technologies), terpineol, polyvinyl butyral (PVB), and isopropanol was deposited by means of the drop-casting technique on a 300 μm thick 8% yttria-stabilized zirconia (8YSZ) planar support. After deposition of the slurry, the sample was dried and then sintered at 1250 °C for 5 h. This method produced a dense NiGDC layer (80 μm thick) on the 8YSZ support with an overall sample diameter of 25 mm. The measurements reported in this study were performed on smaller fragments (≈35 mm^2 area) of the original assembly.

NAP-XPS and NEXAFS were performed at the ISISS (Innovative Station for In-Situ Spectroscopy) beamline at the BESSY II/HZB synchrotron facility (Berlin, Germany).[51] For the measurements, the samples were mounted between two stainless-steel clamps; the top clamp had a slit 4 mm in diameter for spectroscopic measurements, whereas the bottom clamp was heated by using an IR laser. Prior to the measurements, the samples were annealed in 0.2 mbar O_2 until residual carbon was removed from the surface, as confirmed by the NAP-XPS C 1s peak. NAP-XPS spectra were collected by using selected photon energies so that the obtained photoelectrons have the same kinetic energy (180 eV) and thus the same sample information depth (≈1.7 nm).[52] All presented NAP-XPS spectra were recorded by using a photoelectron pass energy of 50 eV. No electrostatic charging was observed under the employed experimental conditions, therefore, the binding energies are presented as measured.

The contributions of metallic Ni, NiO, $CeO_{1.5}$, and CeO_2 to the Ni 2p and Ce 3d spectra were estimated by using a peak-fitting procedure with reference spectra of standard reference samples measured at the same spectrometer. In particular, commercially available CeO_2 and NiO powder samples (Sigma–Aldrich) were pressed into pellets and measured under relevant conditions. Nickel powder, after reduction in H_2 and oxidation in O_2, served as the Ni and NiO standards, respectively. The CeO_2 standard was produced by heating ceria powder in O_2, whereas the Ce 3d reference spectrum for $CeO_{1.5}$ was taken from Ref. [litr30>]. The peak-area ratio was measured after subtraction of a Shirley background and quantitative calculations were performed by taking into account the photon flux photon energy and the photoionization cross-section dependence of the atomic subshells.[53] The stoichiometry of nickel and ceria in the surface region (about 1.7 nm) was estimated from the NAP-XPS spectra by using the formula previously proposed by Henderson et al..[20] In particular, the stoichiometry x for NiO_x was quantified from Equation (1):

$$x = \frac{NiO}{Ni + NiO} \quad (0 \le x \le 1) \qquad (1)$$

whereas that of ceria was calculated from Equation (2):

$$y = \frac{2CeO_2 + 1.5CeO_{1.5}}{CeO_2 + CeO_{1.5}} \quad (1.5 \le y \le 2) \qquad (2)$$

More details are given in Supporting Information 5.

The NEXAFS spectra were recorded in the total electron yield (TEY) mode, enhanced by additional electrons created by ionization of the gas phase above the sample. Photon-beam-damage effects were tested by shifting the analysis spot to a new sample position, and the lack of differences between the spectra demonstrates the stability of the samples under the photon beam in the timeframe of the experiment. The surface morphology was inspected by using scanning electron microscopy (SEM) by using a Jeol JSM-6700F microscope. The SEM images showed a porous surface morphology, characteristic for solid-oxide electrodes, formed from particle agglomerates with sizes of 0.2–1 μm (see Supporting Information 7).

Acknowledgements

The research leading to these results has received funding from the Fuel Cells and Hydrogen 2 Joint Undertaking under the project SElySOs with grant agreement no. 671481. This Joint Undertaking received support from the European Union's Horizon 2020 Research and Innovation Programme and Greece, Germany, Czech Republic, France, and Norway. We thank the Inorganic Chemistry department of the Fritz-Haber-Institut der MPG and, in particular, M. Hävecker, D. Teschner, and A. Knop-Gericke for the opportunity to use the SISS beamline and H.Z.B. for the allocation of synchrotron radiation beamtime. Finally, S.Z. acknowledge financial support from the European Community's Seventh Framework Programme (FP7/2007–2013) under grant agreement no. 312284.

Keywords: cerium · chemical states · electrodes · electrolysis cells · photoelectron spectroscopy · nickel

[1] M. A. Laguna-Bercero, *J. Power Sources* **2012**, *203*, 4–16.
[2] M. Wang, Z. Wang, X. Gong, Z. Guo, *Renewable Sustainable Energy Rev.* **2014**, *29*, 573–588.
[3] K. Yamamoto, N. Qiu, S. Ohara, *Sci. Rep.* **2015**, *5*, 17433.
[4] M. Mogensen, N. M. Sammes, G. A. Tompsett, *Solid State Ionics* **2000**, *129*, 63–94.
[5] K. Yamamoto, T. Hashishin, M. Matsuda, N. Qiu, Z. Tan, S. Ohara, *Nano Energy* **2014**, *6*, 103–108.
[6] B. C. H. Steele, *Solid State Ionics* **2000**, *129*, 95–110.
[7] S. D. Park, J. M. Vohs, R. J. Gorte, *Nature* **2000**, *404*, 265–267.
[8] M. Yoshinaga, H. Kishimoto, K. Yamaji, Y.-P. Xiong, M. E. Brito, T. Horita, H. Yokokawa, *Solid State Ionics* **2011**, *192*, 571–575.
[9] P. Kim-Lohsoontorn, Y.-M. Kim, N. Laosiripojana, J. Bae, *Int. J. Hydrogen Energy* **2011**, *36*, 9420–9427.
[10] V. Singh, H. Muroyama, T. Matsui, S. Hashigami, T. Inagaki, K. Eguchi, *J. Power Sources* **2015**, *293*, 642–648.
[11] Q. Fang, L. Blum, N. H. Menzler, *J. Electrochem. Soc.* **2015**, *162*, F907–F912.
[12] B. Farrell, S. Linic, *Appl. Catal. B* **2016**, *183*, 386–393.
[13] J. Hanna, W. Y. Lee, Y. Shi, A. F. Ghoniem, *Prog. Energy Combust. Sci.* **2014**, *40*, 74–111.
[14] C. Graves, S. D. Ebbesen, M. Mogensen, K. S. Lackner, *Renewable Sustainable Energy Rev.* **2011**, *15*, 1–23.
[15] B. P. Payne, M. C. Biesinger, N. S. McIntyre, *J. Electron Spectrosc. Relat. Phenom.* **2009**, *175*, 55–65.
[16] J. C. de Jesus, J. Carrazza, P. Pereira, F. Zaera, *Surf. Sci.* **1998**, *397*, 34–47.
[17] F. El Gabaly, K. F. McCarty, H. Bluhm, A. H. McDaniel, *Phys. Chem. Chem. Phys.* **2013**, *15*, 8334–8341.
[18] J. Paier, C. Penschke, J. Sauer, *Chem. Rev.* **2013**, *113*, 3949–3985.
[19] D. R. Mullins, *Surf. Sci. Rep.* **2015**, *70*, 42–85.

[20] M. A. Henderson, C. L. Perkins, M. H. Engelhard, S. Thevuthasan, C. H. F. Peden, *Surf. Sci.* **2003**, *526*, 1 – 18.
[21] C. Zhang, M. E. Grass, A. H. McDaniel, S. C. DeCaluwe, F. El Gabaly, Z. Liu, K. F. McCarty, R. L. Farrow, M. A. Linne, Z. Hussain, G. S. Jackson, H. Bluhm, B. W. Eichhorn, *Nat. Mater.* **2010**, *9*, 944 – 949.
[22] Z. A. Feng, F. El Gabaly, X. Ye, Z.-X. Shen, W. C. Chueh, *Nat. Commun.* **2014**, *5* 4374.
[23] J. Carrasco, D. Lopez-Duran, Z. Liu, T. Duchon, J. Evans, S. D. Senanayake, E. J. Crumlin, V. Matolin, J. A. Rodriguez, M. V. Ganduglia-Pirovano, *Angew. Chem. Int. Ed.* **2015**, *54*, 3917 – 3921; *Angew. Chem.* **2015**, *127*, 3989 – 3993.
[24] R. C. Maher, P. R. Shearing, E. Brightman, D. J. L. Brett, N. P. Brandon, L. F. Cohen, *Adv. Sci.* **2016**, *3*, 1500146.
[25] D. R. Mullins, P. M. Albrecht, T.-L. Chen, F. C. Calaza, M. D. Biegalski, H. M. Christen, S. H. Overbury, *J. Phys. Chem. C* **2012**, *116*, 19419 – 19428.
[26] Y. T. Law, T. Skala, I. Pis, V. Nehasil, M. Vondracek, S. Zafeiratos, *J. Phys. Chem. C* **2012**, *116*, 10048 – 10056.
[27] V. V. Kaichev, D. Teschner, A. A. Saraev, S. S. Kosolobov, A. Y. Gladky, I. P. Prosvirin, N. A. Rudina, A. B. Ayupov, R. Blume, M. Haevecker, A. Knop-Gericke, R. Schloegl, A. V. Latyshev, V. I. Bukhtiyarov, *J. Catal.* **2016**, *334*, 23 – 33.
[28] A. Ponchel, A. D'Huysser, C. Lamonier, L. Jalowiecki-Duhamel, *Phys. Chem. Chem. Phys.* **2000**, *2*, 303 – 312.
[29] M. Abbate, J. B. Goedkoop, F. M. F. Degroot, M. Grioni, J. C. Fuggle, S. Hofmann, H. Petersen, M. Sacchi, *Surf. Interface Anal.* **1992**, *18*, 65 – 69.
[30] V. Papaefthimiou, M. Shishkin, D. K. Niakolas, M. Athanasiou, Y. T. Law, R. Arrigo, D. Teschner, M. Haevecker, A. Knop-Gericke, R. Schloegl, T. Ziegler, S. G. Neophytides, S. Zafeiratos, *Adv. Energy Mater.* **2013**, *3*, 762 – 769.
[31] A. P. Grosvenor, M. C. Biesinger, R. S. Smart, N. S. McIntyre, *Surf. Sci.* **2006**, *600*, 1771 – 1779.
[32] D. R. Mullins, S. H. Overbury, D. R. Huntley, *Surf. Sci.* **1998**, *409*, 307 – 319.
[33] S. Luo, N.-P. Thuy-Duong, A. C. Johnston-Peck, L. Barrio, S. Sallis, D. A. Arena, S. Kundu, W. Xu, L. F. J. Piper, E. A. Stach, D. E. Polyansky, E. Fujita, J. A. Rodriguez, S. D. Senanayake, *J. Phys. Chem. C* **2015**, *119*, 2669 – 2679.
[34] G. Zhou, P. R. Shah, T. Montini, P. Fornasiero, R. J. Gorte, *Surf. Sci.* **2007**, *601*, 2512 – 2519.
[35] J. Liu, X. Tian, H. Chen, Y. Shao, G. Yang, D. Chen, *Appl. Surf. Sci.* **2015**, *348*, 60 – 65.
[36] L. Zheng, X. Cheng, D. Cao, D. Zhang, Z. Wang, D. Xu, C. Xia, L. Shen, Y. Yu, *RSC Adv.* **2014**, *4*, 44296 – 44301.
[37] V. Matolin, I. Matolinova, F. Dvorak, V. Johanek, J. Myslivecek, K. C. Prince, T. Skala, O. Stetsovych, N. Tsud, M. Vaclavu, B. Smid, *Catal. Today* **2012**, *181*, 124 – 132.
[38] W. C. Chueh, A. H. McDaniel, M. E. Grass, Y. Hao, N. Jabeen, Z. Liu, S. M. Haile, K. F. McCarty, H. Bluhm, F. El Gabaly, *Chem. Mater.* **2012**, *24*, 1876 – 1882.
[39] Y. Wang, A. Zhu, Y. Zhang, C. T. Au, X. Yang, C. Shi, *Appl. Catal. B* **2008**, *81*, 141 – 149.
[40] K. V. Manukyan, A. G. Avetisyan, C. E. Shuck, H. A. Chatilyan, S. Rouvimov, S. L. Kharatyan, A. S. Mukasyan, *J. Phys. Chem. C* **2015**, *119*, 16131 – 16138.
[41] W. S. M. Werner, M. Chudzicki, W. Smekal, C. J. Powell, *Appl. Phys. Lett.* **2014**, *104*.
[42] H. Kuipers, H. C. E. Vanleuven, W. M. Visser, *Surf. Interface Anal.* **1986**, *8*, 235 – 242.
[43] Z.-P. Li, T. Mori, G. J. Auchterlonie, Y. Guo, J. Zou, J. Drennan, M. Miyayama, *J. Phys. Chem. C* **2011**, *115*, 6877 – 6885.
[44] F. S. Torknik, M. Keyanpour-Rad, A. Maghsoudipour, G. M. Choi, *Ceram. Int.* **2014**, *40*, 1341 – 1350.
[45] J. L. F. Da Silva, *Phys. Rev. B* **2007**, *76*.
[46] M. Alsabet, M. Grden, G. Jerkiewicz, *Electrocatalysis* **2014**, *5*, 136 – 147.
[47] S. Zafeiratos, F. Paloukis, G. Papakonstantinou, D. Teschner, M. Havecker, E. Vass, P. Schnorch, A. Knop-Gericke, R. Schlogl, B. Moreno, E. Chinarro, J. R. Jurado, S. G. Neophytides, *Catal. Today* **2010**, *157*, 250 – 256.
[48] H. A. Hansen, C. Wolverton, *J. Phys. Chem. C* **2014**, *118*, 27402 – 27414.
[49] D. K. Niakolas, J. P. Ouweltjes, G. Rietveld, V. Dracopoulos, S. G. Neophytides, *Int. J. Hydrogen Energy* **2010**, *35*, 7898 – 7904.
[50] C. Neofytidis, M. Athanasiou, S. G. Neophytides, D. K. Niakolas, *Top. Catal.* **2015**, *58*, 1276 – 1289.
[51] A. Knop-Gericke, E. Kleimenov, M. Haevecker, R. Blume, D. Teschner, S. Zafeiratos, R. Schloegl, V. I. Bukhtiyarov, V. V. Kaichev, I. P. Prosvirin, A. I. Nizovskii, H. Bluhm, A. Barinov, P. Dudin, M. Kiskinova, *Adv. Catal.* **2009**, *52*, 213 – 272.
[52] S. Tanuma, C. J. Powell, D. R. Penn, *Surf. Interface Anal.* **1994**, *21*, 165 – 176.
[53] J. J. Yeh, I. Lindau, *At. Data Nucl. Data Tables* **1985**, *32*, 1 – 155.

Manuscript received: August 26, 2016
Accepted Article published: October 28, 2016
Final Article published: November 22, 2016